CHINESE OPTICS LETTERS

Vol. 19, No. 7 | July 2021

Self-aligned fiber-based dual-beam source for STED nanolithography

Jian Chen (陈 建), Guoliang Chen (陈国梁), and Qiwen Zhan (詹其文)*

School of Optical-Electrical and Computer Engineering, University of Shanghai for Science and Technology, Shanghai 201800, China

*Corresponding author: qwzhan@usst.edu.cn

Received September 3, 2020 | Accepted December 5, 2020 | Posted Online March 18, 2021

A fiber-based source that can be exploited in a stimulated emission depletion (STED) inspired nanolithography setup is presented. Such a source maintains the excitation beam pulse, generates a ring-shaped depletion beam, and automatically realizes dual-beam coaxial alignment that is critical for two beam nanolithography. The mode conversion of the depletion beam is realized by using a customized vortex fiber, which converts the Gaussian beam into a donut-shaped azimuthally polarized beam. The pulse width and repetition frequency of the excitation beam remain unchanged, and its polarization states can be controlled. According to the simulated point spread function of each beam in the focal region, the full width at half-maximum of the effective spot size in STED nanofabrication could decrease to less than 28.6 nm.

Keywords: nanolithography; vortex fiber; direct laser writing; STED; controlled fabrication.

DOI: 10.3788/COL202119.072201

1. Introduction

Nanolithography is playing an increasingly important role in modern society. However, due to the limitation of Abbe's diffraction, the feature size by single-beam lithography cannot exceed half a wavelength. Inspired by stimulated emission depletion (STED) microscopy[1], which has been widely used in micro-imaging[2], dual-beam STED lithography has become a simple and effective way to break through the diffraction limit. The main principle is that the hollow depletion beam can inhibit the polymerization reaction between the excitation beam and the photosensitive material, and only the hollow part in the middle allows the excitation beam for direct laser writing, thereby realizing lithography that breaks the diffraction limit[3]. Since STED lithography can easily realize arbitrary two-dimensional (2D) or three-dimensional (3D) structures[4], it would be highly desirable in biotechnology[5,6] and photonic devices[7–11]. The STED microscope technique was firstly used in photolithography to achieve a linewidth of 65 nm by Fischer *et al.*[12]. With the optimization of the STED lithography structure[13,14] and the improvement of inhibitors and initiators[15–17], the linewidth of dual-beam lithography technology has been significantly reduced. For example, Gan *et al.* successfully demonstrated 9 nm linewidth processing[18]. The traditional spatial STED lithography system has high requirements for dual-beam alignment and device stability, while optical fibers are the most promising candidate to overcome these issues. The optical fiber can be used to generate and transmit the donut-shaped depletion beam, while maintaining the characteristics of the pulsed excitation beam at a different wavelength. Due to the self-alignment of the optical fiber[19–21], the excitation and depletion beams are completely overlapped with each other. The fiber-based STED nanolithography system guarantees the coaxial alignment of the two beams and ensures system stability, which significantly improve the practicality of the STED nanolithography.

In this article, a customized vortex fiber is used to generate and coaxially align the depletion beam and the excitation beam employed in STED nanolithography. More details of the vortex fiber can be found in Refs. [22,23]. The lasers with wavelengths of 1030 nm and 532 nm are coupled into the vortex fiber simultaneously. The near-infrared pulsed laser is usually used as the excitation beam source in lithography technology, which is mainly due to the low photon energy in this wavelength range and good penetrability of materials. The continuous-wave (CW) 532 nm fundamental Gaussian mode is converted into ring-shaped TE_{01} mode by the vortex fiber, which is adopted as the depletion beam for STED lithography. Meanwhile, the vortex fiber maintains the characteristics of a pulsed 1030 nm fundamental mode with controllable polarization as the excitation beam for STED lithography. With the self-alignment provided by the fiber, it is simple to maintain the two beams to be strictly coaxial. The Stokes parameter measurement for the two beams are used to simulate point spread function (PSF) of each beam within the focal region and calculate the effective spot size for the dual-beam STED nanofabrication.

2. Experiments

The schematic diagram of fiber-based STED nanolithography setup is shown in Fig. 1. A home-built fiber laser[24,25] is employed to generate a pulse laser with a central wavelength of 1030 nm, whose polarization is adjusted with a half-wave plate (HWP). The polarization of the 532 nm CW laser is controlled by an HWP and a quarter-wave plate. The dichroic mirror (DMLP805, Thorlabs) is used to transmit the 1030 nm beam and reflect the 532 nm beam, and the two beams are brought to roughly coincide in space by adjusting the propagation directions of the two beams with mirror pairs. The carefully selected lens L is exploited to focus both of them into a spot size of about 2 μm, which is equivalent to the core size of the vortex fiber. The nanometer translation stage (NanoMax 300, Thorlabs) is used to adjust the position of the optical fiber so that two beams can be coupled into the single-mode fiber at the same time with high efficiency.

The single-mode fiber transmits two beams to the Bragg grating, which converts the 532 nm laser into high-order modes while maintaining the 1030 nm laser in the fundamental mode. The Bragg grating couples two beams into the vortex fiber with the refractive index of its core in ring-shaped distribution. This customized fiber could increase the effective refractive index difference between adjacent high-order modes, realizing the generation of a polarization vortex beam. An azimuthally polarized 532 nm beam (TE_{01} mode) is selected by the tilted long-period grating in the vortex fiber, while the intensity distribution of 1030 nm laser is maintained as unchanged. Subsequently, the 1030 nm Gaussian mode pulsed laser is utilized as an excitation beam, and the donut-shaped 532 nm laser is exploited as the depletion beam required by STED lithography. Due to the self-alignment offered by the optic fiber, the output excitation beam and depletion beam are strictly coaxial.

3. Results and Discussion

First, we block the 532 nm laser and adjust the 1030 nm beam to vertical polarization by rotating the HWP. A quarter-wave plate and a polarizer are placed behind the fiber tail to measure the Stokes parameters of the excitation beam with the power of 6 mW. The polarization, frequency spectrum, pulse sequence, and pulse width of the excitation beam are measured in front of and behind the vortex fiber to check whether the fiber will cause any changes to the laser pulse. The measured results are shown in Figs. 2 and 3. According to the comparison between Figs. 2(a) and 2(b), the intensity distribution of the 1030 nm beam is still the Gaussian distribution, but its polarization is changed from the vertical to horizontal direction. The spectrum width of the input pulsed beam is about 20 nm, and its central wavelength is 1030 nm [Fig. 2(c)]. The spectrum of the output beam after the vortex fiber remains almost unchanged, and the central wavelength is still 1030 nm [Fig. 2(d)]. According to the measured input and output pulse sequences [Figs. 3(a) and 3(b)], the repetition frequency of 1030 nm laser remains consistent at 52.6 MHz. From Fig. 3(c), we can see that the pulse width of the 1030 nm laser is 1.2 ps. The experiments prove that

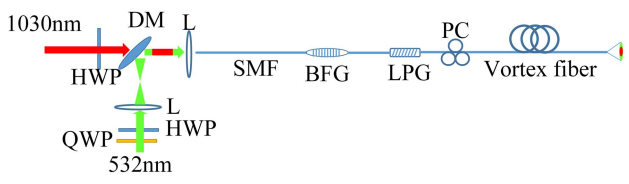

Fig. 1. Schematic diagram of fiber-based STED nanolithography setup. (HWP, half wave plate; QWP, quarter wave plate; DM, dichroic mirror; L, lens; SMF, single-mode fiber; BFG, Bragg fiber grating; LPG, long-period grating; PC, polarization controller.)

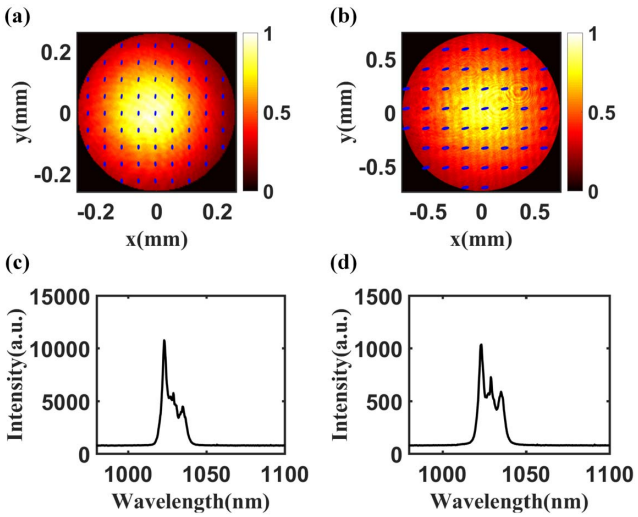

Fig. 2. (a) Intensity and polarization distributions of 1030 nm input laser in front of the vortex fiber (the ellipses represent the direction of polarization). (b) Intensity and polarization distributions of 1030 nm output laser behind the fiber tail. Spectra of 1030 nm laser (c) in front of and (d) behind the fiber.

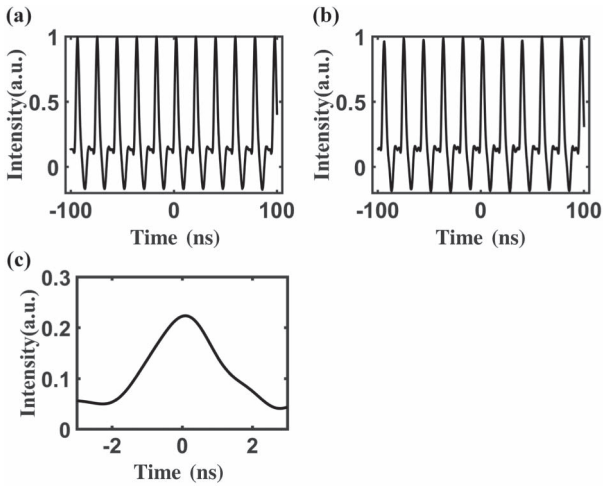

Fig. 3. Pulse sequences of 1030 nm laser (a) in front of and (b) behind the fiber. (c) Pulse width of excitation beam.

the vortex fiber brings negligible changes to the characteristics of the pulsed 1030 nm laser. Thus, the 1030 nm laser transmitted by the vortex fiber can be used as the excitation beam for STED lithography. Meanwhile, it is found that the polarization of the output beam is orthogonal to the incident polarization state. Using these polarization transmission characteristics of the vortex fiber, the polarization of the excitation beam can be adjusted through controlling the input polarization prior to coupling into the vortex fiber. This may allow for a better match to the polarization of the depletion beam and improve the linewidth of the lithography beyond the diffraction limit[26].

Then, we block the 1030 nm laser and adjust the polarization state of the incident 532 nm laser coupled to the vortex fiber to produce a ring-shaped output beam. The polarizer placed behind the vortex fiber is employed to qualitatively reveal the polarization pattern of the output beam, as shown in Fig. 4(a). The white arrow indicates the transmission axis of the polarizer. The intensity and polarization state distribution of the ring-shaped beam are quantitatively reconstructed by using the measured Stokes parameters, as shown in Fig. 4(b). The polarization of the output beam is axially symmetric and along the azimuthal direction, while the intensity distribution is in a donut shape. All of the above results prove that the output beam is the TE_{01} mode (i.e., azimuthally polarized beam), which can be used as the depletion beam for STED lithography.

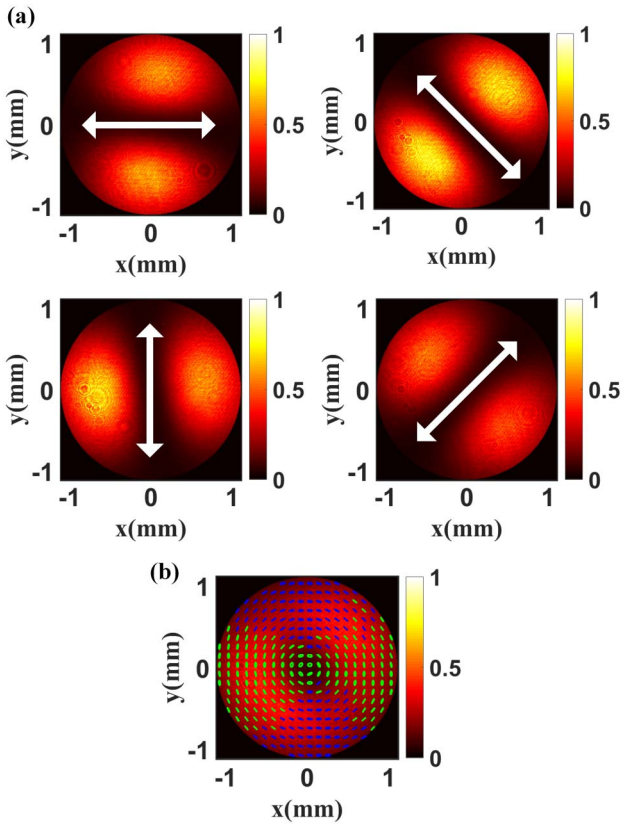

Fig. 4. (a) Output 532 nm laser after passing through a linear polarizer with different transmission axis orientations. (b) Intensity and polarization distributions of 532 nm laser behind the fiber tail.

Subsequently, the reconstructed field obtained by the Stokes parameters is employed to simulate the focused depletion beam PSF with the Richard–Wolf vectorial diffraction theory, as the following[27–30]:

$$\boldsymbol{E} = \frac{j}{\lambda}\int_0^{\theta_{\max}}\int_0^{2\pi} \boldsymbol{E}_o(\theta,\varphi) \times e^{jkr_p \sin\theta\cos(\varphi-\phi)+jkz_p\cos\theta} \sin\theta \mathrm{d}\theta\mathrm{d}\varphi, \tag{1}$$

where $\boldsymbol{E}_o(\theta,\varphi)$ is the pupil field of a lens with high numerical aperture (NA). In the following simulations, an NA of 0.9 will be used. The simulation results of the depletion beam PSF in the xy plane in the focal region are shown in Fig. 5(a). The full width at half-maximum (FWHM) of the hollow center in the depletion beam PSF is about 202 nm.

An amplification system is built by using a high NA objective lens (NA = 0.9, 100 ×) and lens L to observe the tightly focused depletion beam PSF, as shown in Fig. 5(b). The mirror M is placed at the focal plane of the objective lens. The experimentally measured depletion beam PSF on the focal plane is shown in Fig. 5(c), from which the FWHM of the hollow center is estimated to be 226 nm by considering the amplification factor of 92. The experimental value is close to the simulated result. The discrepancy is mainly attributed to the limited precision of stages, the accuracy of the field measurement at the pupil plane, etc.

Similarly, the simulation results of the excitation beam PSF in the xy plane are shown in Fig. 6(a). The FWHMs of the excitation beam are found to be about 494 nm along the y direction, and about 680 nm along the x direction. The excitation beam PSF and depletion beam PSF overlapped in the xy plane; therefore, the effective beam intensity I_{fl} during the STED nanolithography process can be expressed as[31,32]

$$I_{\mathrm{fl}} = I_{\mathrm{exc}} \exp(-\alpha\sigma I_{\mathrm{sted}}), \tag{2}$$

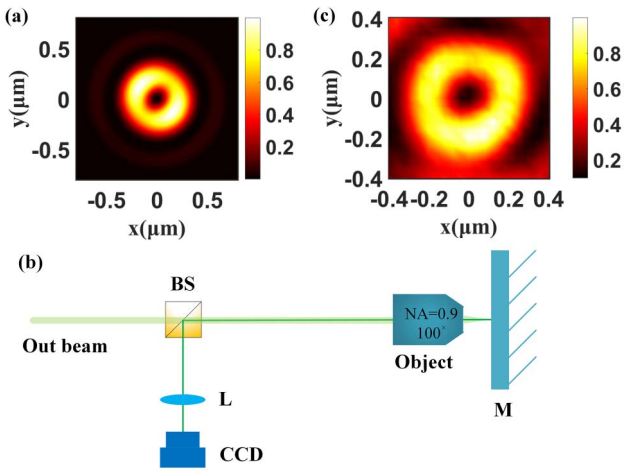

Fig. 5. (a) Simulated depletion beam PSF in the xy plane of the focal region. (b) Focus amplification system (BS, beam splitter; L, lens; M, mirror). (c) Experimentally measured focused depletion beam PSF.

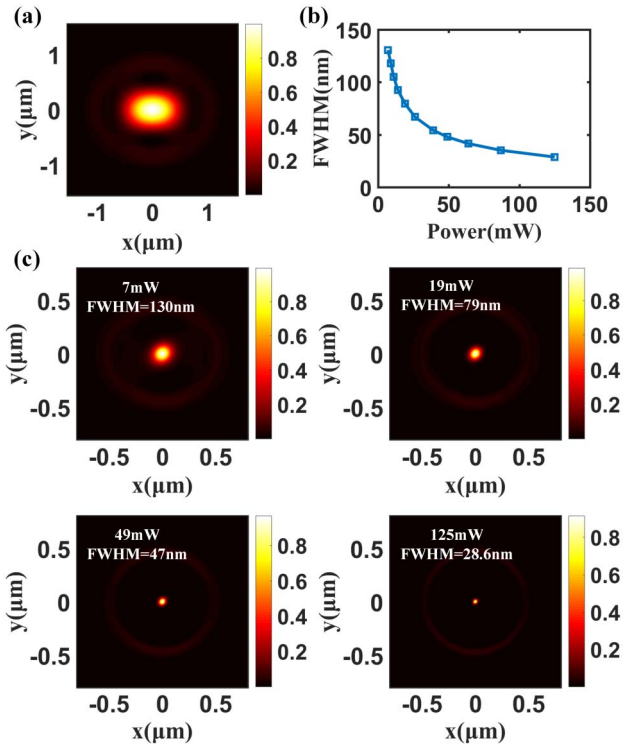

Fig. 6. (a) Simulated excitation beam PSF and (b) relationship between the FWHM of the effective beam and the power of the depletion beam in the *xy* plane of the focal region. (c) Intensity distribution of the effective beam in the *xy* plane of the focal region under different depletion beam powers.

where I_{exc} and I_{sted} are the intensities of the excitation beam and depletion beam, respectively. $\alpha = |\boldsymbol{E}_{\text{exc}} \cdot \boldsymbol{E}_{\text{sted}}| / \sqrt{I_{\text{exc}} \cdot I_{\text{sted}}}$, and σ is the size of the cross section of the stimulated emission. We maintain the power of the excitation beam as 6 mW, while adjusting the power of the depletion beam. The relationship between the effective FWHM and the power of the depletion beam in the *xy* plane of the focal region is shown in Fig. 6(b). As the power of the depletion beam increases, the FWHM of the effective beams continuously decreases. The intensity distributions of the effective beams at several different power levels through simulation are also depicted in Fig. 6(c). Obviously, because of the composite effect of the two beams, the intensity of the effective beam is much smaller than that of the excitation beam. The effective FWHM for STED nanolithography is about 28.6 nm when the power of the depletion beam reaches 125 mW. In fact, the threshold of the depletion beam is related to photoresist. According to Refs. [12,15], the power of the depletion beam could exceed 100 mW, so the maximum power of the depletion beam is set as 125 mW in the simulations. This suggests that STED lithography using this fiber-based dual-beam source could be capable of breaking the diffraction limit.

4. Conclusion

A fiber-based source that is suitable for STED nanolithography is presented, which can generate an excitation beam and a donut-shaped depletion beam required by STED lithography. Such a fiber-based source maintains strictly coaxial alignment for the dual-beam setup. The experimental results indicate that the pulse width, spectrum, and repetition frequency remain unchanged when a pulsed beam with a central wavelength of 1030 nm passes through the system, which can serve as the excitation beam for STED lithography. The polarization of the excitation beam can be controlled to match with the polarization of the depletion beam, leading to improvement of the linewidth in direct laser writing. The mode of the 532 nm continuous laser is selected through the vortex fiber, and a donut-shaped azimuthally polarized beam is produced as the depletion beam of STED lithography. The measured Stokes parameters are carried out to quantitatively reveal the polarization and intensity distributions of the beams generated by the vortex fiber. Using the Richard–Wolf vector diffraction theory, the excitation beam and depletion beam PSFs in the focal region are simulated, and the effective beam in STED nanofabrication is analyzed. The effective FWHM decreases continuously as the power of the depletion beam increases, which provides the capability to break the diffraction limit. Compared with traditional STED lithography, fiber-based STED lithography is simpler, more stable, and easier to be integrated and miniaturized, which may be widely exploited in the field of micromachining.

Acknowledgement

This work was supported by the National Natural Science Foundation of China (No. 61805142), the Shanghai Science and Technology Committee (No. 19060502500), and the Natural Science Foundation of Shanghai (No. 20ZR1437600).

References

1. S. W. Hell and J. Wichmann, "Breaking the diffraction resolution limit by stimulated emission: stimulated-emission-depletion fluorescence microscopy," Opt. Lett. **19**, 780 (1994).
2. J. Du, S. Deng, S. Hou, L. Qiao, J. Chen, Q. Huang, C. Fan, Y. Cheng, and Y. Zhao, "Superresolution imaging of DNA tetrahedral nanostructures in cells by STED method with continuous wave lasers," Chin. Opt. Lett. **12**, 041101 (2014).
3. T. A. Klar, R. Wollhofen, and J. Jacak, "Sub-Abbe resolution: from STED microscopy to STED lithography," Phys. Scripta **2014**, 014049 (2014).
4. Y. L. Zhang, Q. D. Chen, H. Xia, and H. B. Sun, "Designable 3D nanofabrication by femtosecond laser direct writing," Nano. Today **5**, 435 (2010).
5. M. Wiesbauer, R. Wollhofen, B. Vasic, K. Schilcher, J. Jacak, and T. A. Klar, "Nano-anchors with single protein capacity produced with STED lithography," Nano. Lett. **13**, 5672 (2013).
6. J. Fischer and M. Wegener, "Three-dimensional optical laser lithography beyond the diffraction limit," Laser Photon. Rev. **7**, 22 (2013).
7. X. He, T. Li, J. Zhang, and Z. Wang, "STED direct laser writing of 45 nm width nanowire," Micromachines **10**, 726 (2019).
8. T. Jiang, S. Gao, Z. Tian, H. Zhang, and L. Niu, "Fabrication of diamond ultra-fine structures by femtosecond laser," Chin. Opt. Lett. **18**, 101402 (2020).
9. B. Buchegger, J. Kreutzer, B. Plochberger, R. Wollhofen, D. Sivun, J. Jacak, G. J. Schütz, U. Schubert, and T. A. Klar, "Stimulated emission depletion lithography with mercapto-functional polymers," ACS Nano **10**, 1954 (2016).

10. J. Kaschke and M. Wegener, "Gold triple-helix mid-infrared metamaterial by STED-inspired laser lithography," Opt. Lett. **40**, 3986 (2015).
11. M. Deubel, G. von Freymann, M. Wegener, S. Pereira, K. Busch, and C. M. Soukoulis, "Direct laser writing of three-dimensional photonic-crystal templates for telecommunications," Nat. Mater. **3**, 444 (2004).
12. J. Fischer, G. von Freymann, and M. Wegener, "The materials challenge in diffraction-unlimited direct-laser-writing optical lithography," Adv. Mater. **22**, 3578 (2010).
13. L. Li, R. R. Gattass, E. Gershgoren, H. Hwang, and J. T. Fourkas, "Achieving $\lambda/20$ resolution by one-color initiation and deactivation of polymerization," Science **324**, 910 (2009).
14. Z. B. Sun, X. Z. Dong, W. Q. Chen, S. Nakanishi, X. M. Duan, and S. Kawata, "Multicolor polymer nanocomposites: *in situ* synthesis and fabrication of 3D microstructures," Adv. Mater. **20**, 914 (2008).
15. T. F. Scott, B. A. Kowalski, A. C. Sullivan, C. N. Bowman, and R. R. McLeod, "Two-color single-photon photoinitiation and photoinhibition for subdiffraction photolithography," Science **324**, 913 (2009).
16. H. Xia, S. Yang, L. Wang, J. Zhao, C. Xue, Y. Wu, and R. Tai, "Nonuniform self-imaging of achromatic Talbot lithography," Chin. Opt. Lett. **17**, 062201 (2019).
17. J. Fischer, J. B. Mueller, A. S. Quick, J. Kaschke, C. Barner-Kowollik, and M. Wegener, "Exploring the mechanisms in STED-enhanced direct laser writing," Adv. Opt. Mater. **3**, 221 (2015).
18. Z. Gan, Y. Cao, R. A. Evans, and M. Gu, "Three-dimensional deep sub-diffraction optical beam lithography with 9 nm feature size," Nat. Commun. **4**, 2061 (2013).
19. M. Gu, H. Kang, and X. Li, "Breaking the diffraction-limited resolution barrier in fiber-optical two-photon fluorescence endoscopy by an azimuthally-polarized beam," Sci. Rep. UK **4**, 3627 (2014).
20. D. Wildanger, J. Bückers, V. Westphal, S. W. Hell, and L. Kastrup, "A STED microscope aligned by design," Opt, Express **17**, 16100 (2009).
21. L. Yan, P. Kristensen, and S. Ramachandran, "Vortex fibers for STED microscopy," APL Photon. **4**, 022903 (2019).
22. S. Ramachandran and P. Kristensen, "Optical vortices in fiber," Nanophotonics **2**, 455 (2013).
23. S. Ramachandran, P. Kristensen, and M. F. Yan, "Generation and propagation of radially polarized beams in optical fibers," Opt. Lett. **34**, 2525 (2009).
24. A. Chong, L. G. Wright, and F. W. Wise, "Ultrafast fiber lasers based on self-similar pulse evolution: a review of current progress," Rep. Prog. Phys. **78**, 113901 (2015).
25. C. Y. Chong, J. Buckley, and F. Wise, "All-normal-dispersion femtosecond fiber laser," Opt. Express **14**, 10095 (2006).
26. Y. Xue, C. Kuang, X. Hao, Z. Gu, and X. Liu, "A method for generating a three-dimensional dark spot using a radially polarized beam," J. Opt. **13**, 125704 (2011).
27. J. Chen, C. Wan, L. Kong, and Q. Zhan, "Experimental generation of complex optical fields for diffraction limited optical focus with purely transverse spin angular momentum," Opt. Express **25**, 8966 (2017).
28. Q. Zhan and J. R. Leger, "Focus shaping using cylindrical vector beams," Opt. Express **10**, 324 (2002).
29. Q. Zhan, "Cylindrical vector beams: from mathematical concepts to applications," Adv. Opt. Photon. **1**, 1 (2009).
30. J. Chen, C. Wan, L. J. Kong, and Q. W. Zhan, "Tightly focused optical field with controllable photonic spin orientation," Opt. Express **25**, 19517 (2017).
31. P. Török and P. R. T. Munro, "The use of Gauss–Laguerre vector beams in STED microscopy," Opt. Express **12**, 3605 (2004).
32. M. Dyba and S. W. Hell, "Focal spots of size $\lambda/23$ open up far-field florescence microscopy at 33 nm axial resolution," Phys. Rev. Lett. **88**, 163901 (2002).